Nuclear Instruments and Methods in Physics Research A 735 (2014) 349–365

Contents lists available at ScienceDirect

Nuclear Instruments and Methods in Physics Research A

journal homepage: www.elsevier.com/locate/nima

Analysis of the wake field effects in the PEP-II storage rings with extremely high currents

A. Novokhatski *, J. Seeman, M. Sullivan

SLAC National Accelerator Laboratory, Stanford University, Menlo Park, CA 94025, USA

ARTICLE INFO

Article history:
Received 13 September 2013
Accepted 13 September 2013
Available online 27 September 2013

Keywords:
Wake fields
Higher order modes
RF heating
Beam instabilities

ABSTRACT

We present the history and analysis of different wake field effects throughout the operational life of the PEP-II SLAC B-factory. Although the impedance of the high and low energy rings is small, the intense high-current beams generated a lot of power. The effects from these wake fields are: heating and damage of vacuum beam chamber elements like RF seals, vacuum valves, shielded bellows, BPM buttons and ceramic tiles; vacuum spikes, vacuum instabilities and high detector background; and beam longitudinal and transverse instabilities. We also discuss the methods used to eliminate these effects. Results of this analysis and the PEP-II experience may be very useful in the design of new storage rings and light sources.

1. Introduction

Intensity dependent effects play an important role in the operation of high luminosity colliders. The SLAC PEP-II asymmetric B-factory storage ring collider nominally collided 1700 bunches of 3.0 A of 3.1 GeV positrons on 1.75 A of 9.0 GeV electrons consisting of a low-energy positron storage ring (LER) situated above a high-energy electron storage ring (HER). The rings intersect at an interaction point (IP) within the BaBar detector sustaining a luminosity of $1.2 \times 10^{34}\,\mathrm{cm}^{-2}\,\mathrm{s}^{-1}$ at the Y(4S) resonance. Achieving this high luminosity was partially due to the increase of operating currents [1]. The high current positron beam holds the record for the number of anti-matter particles stored: 1.5×10^{14}.

Higher current means more power in coherent and incoherent radiation. At the end of the PEP-II run the LER current was increased to a new world record of 3.2 A. During the energy scan, synchrotron radiation power in the high-energy ring exceeded the level of 10 MW in continuous operation, at or near the world record for a lepton storage ring. This large amount of power, produced by 11 RF stations was captured by the wall of the Cu vacuum chamber and then was carefully taken out by a water-cooling system. Additionally to large incoherent radiation, we got bursts of coherent radiation in the form of wake fields.

The design of the PEP-II beam chamber was very challenging. We used shielded bellows and shielded vacuum valves, which had water-cooled flanges. The transitions from elliptical cross-section to circular cross-section were long and smooth. Masks in the interaction region were smoothed. Collimators were designed in a way not to produce longitudinal fields. In order to watch for possible heating of the beam chamber elements, we installed many thermocouples around the ring.

The history of the wake field effects started almost from the very beginning of PEP-II operation.

2. Tiny vertex bellows and a large BABAR detector

High order mode (HOM) heating was observed in the PEP-II interaction region vacuum system [2]. The interaction region vacuum chamber brings the two ring vacuum chambers into a common chamber. In a particular region both beams (LER and HER) excite traveling wake fields or trapped Higher Order Modes (HOMs), which may interfere with each other depending on the beam phases.

The interaction point (IP) has a vertex chamber 50 mm in diameter and 400 mm long. It is a double walled Be chamber with water-cooling to remove induced HOM power. It is connected to a RF shielded bellows that connects to a larger chamber made of Glidcop and Cu. It is also designed to absorb synchrotron radiation with masks that necessitate bumps in the vacuum surface.

One thermocouple (Fig. 1), located near the vertex bellows showed higher readings than expected and caused concern about excessive heating in that region.

* Corresponding author.
E-mail address: novo@slac.stanford.edu (A. Novokhatski).

0168-9002/$ - see front matter © 2013 Elsevier B.V. All rights reserved.
http://dx.doi.org/10.1016/j.nima.2013.09.039

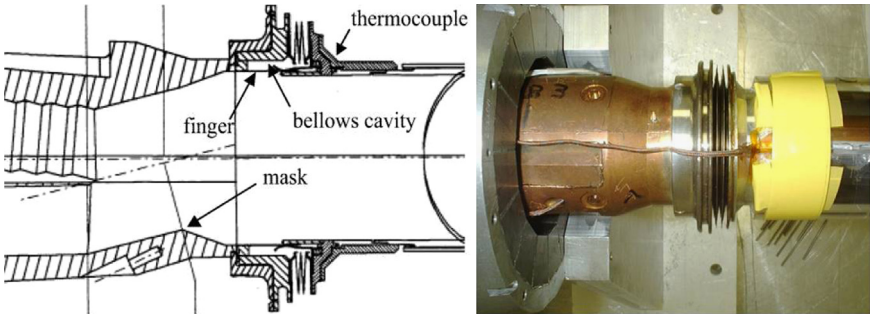

Fig. 1. Vertex bellows in interaction region.

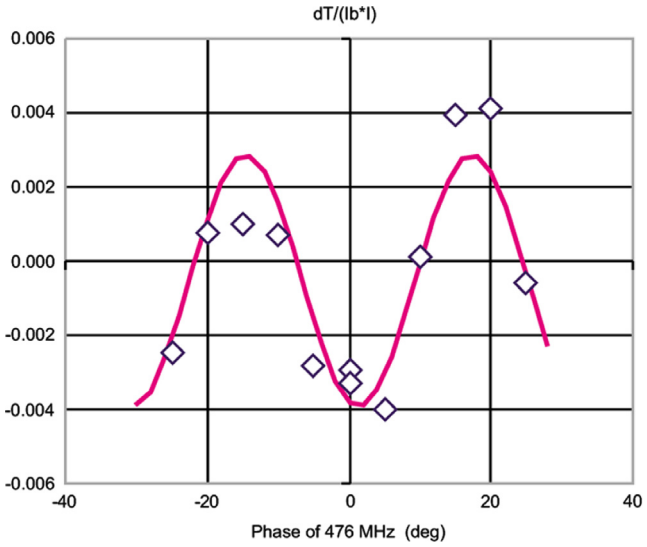

Fig. 2. Modulation of heating by changing the phase of the electron beam. The curve corresponds to 5.4 GHz.

With beam currents of 0.8 A (e^-), on 1.5 A (e^+), at this time, it typically read 150 F, a rise of 90 F above the cooling water temperature. To determine if any single HOM resonance was responsible for the heating, the RF phase of the HER was then moved relative to the LER and a modulation of the temperature was measured (Fig. 2).

We also measured the spectrum of the fields generated in the interaction region using signals from a BPMs located 50 cm from the bellows. We found one mode at the frequency of 5.59 GHz, the power of which was correlated (Fig. 3) with the bellows heating power, which we calculated from the bellows temperature *T*. We estimate the heating power by a formula.

$$P \approx K(T - T_c + \frac{\tau_c}{2}\frac{\partial}{\partial t}T)$$

T_c is a bellows temperature at zero currents, τ_c is a cooling time of an exponential temperature decay, measured after the beams abort. *K* is a constant, which can be estimated from the total power, which is removed from the Be beam pipe. The correlation between amplitude of RF mode and estimated power is shown at Fig. 4. The complicated shape is due to the change of the beam (electron and positron) currents.

Thermocouples on the water exit pipes and knowledge of the flow rates gave an estimate of the power removed from the vertex Be chamber. This estimate was around 600 W for the currents noted above. With simple temperature measurements, we were able to determine the nature of heating in a particular region of the interaction region vacuum system. The current dependence identifies HOM as the source of heat. The response to RF voltage

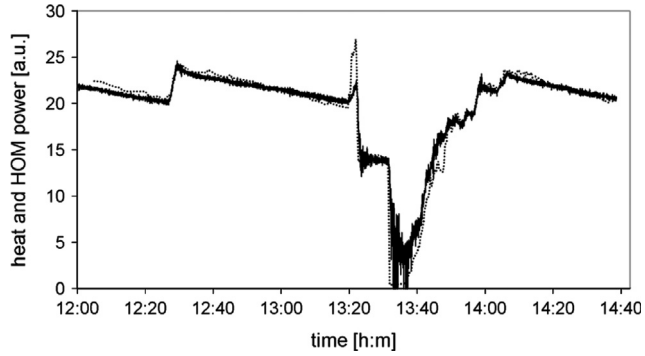

Fig. 3. History correlation of the power of the 5.59 GHz mode (dotted line) and the heat power (solid line), calculated from the bellows temperature.

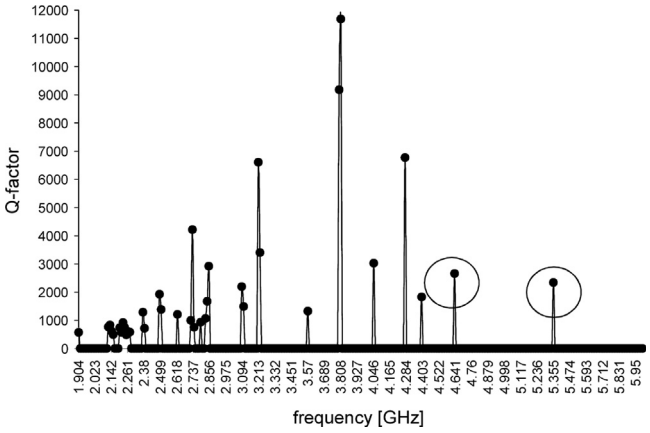

Fig. 4. Q-values of trapped modes at interaction region, measured from the BPM button signal in the time gap between bunch trains. The circled peaks show amplitude correlation the thermocouple temperature.

shows the expected bunch length sensitivity and quadratic relation with the beam currents.

We also measured the Q-value of HOMs, trapped in the interaction region using a gated spectrum analyzer. The gated signal coincides with the time gap where no beam is present and the amplitudes exponentially decay. To calculate the equivalent Q-factor of the modes we measured mode amplitudes in a small time window at the beginning and the end of the gap. We found a Q-value of the interesting mode of order of 2500. We also found another mode at 4.6 GHz, which may be correlated with a beam chamber trapped mode located near the vertex bellows.

We also did a computer analysis [3] of the cavity behind the fingers of vertex bellows and found a resonant dipole mode of 5.46 GHz, which is very close to the measured value. The calculated field distribution in a cavity is shown in Fig. 5 (left plot). The maximum heating (red color) was at the convolution edges just near the place where the convolutions are welded. We also found

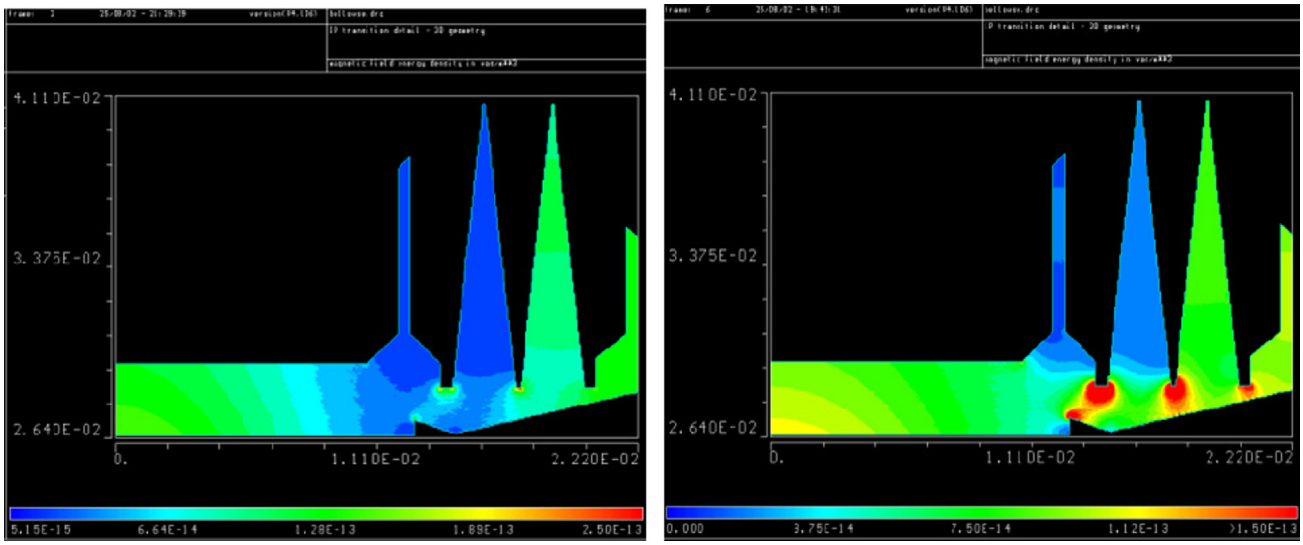

Fig. 5. Field distribution inside a bellows cavity for dipole (left) and quadroupole (right) modes. Red color corresponds to a higher field; blue color corresponds to a smaller field. Green is in the middle, as it shown under the plot. (For interpretation of the references to color in this figure legend, the reader is referred to the web version of this article.)

a quadrupole mode with a frequency of 6.19 GHz, which produces more heating at the convolutions (Fig. 4, right plot).

It is interesting to note that the other vertex bellows situated at the other side of the Be chamber did not show a large rise in temperature. This may be because the vacuum chamber near that bellows had a much smoother design. In order to understand how the vertex bellows cavity can be excited we made a computer model of the interaction region, which is shown in Fig. 6.The synchrotron radiation mask (grooves) worked like a mode transformer of the symmetric bunch field into dipole, quadrupole and other azimuthal harmonics. Some trapped modes in the beam chamber were observed in Omeg3P calculations [4].

There was a large concern that this heat may destroy the convolution welding. In 2003 we opened the BaBar detector and installed more cooling around the vertex bellows. This helped and we did not have further problems in this location even at higher currents. Nevertheless, we designed a bellows replacement, which can survive much higher currents [5]. This bellows contains water-cooled absorbing ceramic tiles, which strongly damp the Q-value of the modes excited in the bellows cavity and may take more than 2 kW power outside the bellows cavity at the projected 3–4 A beam currents.

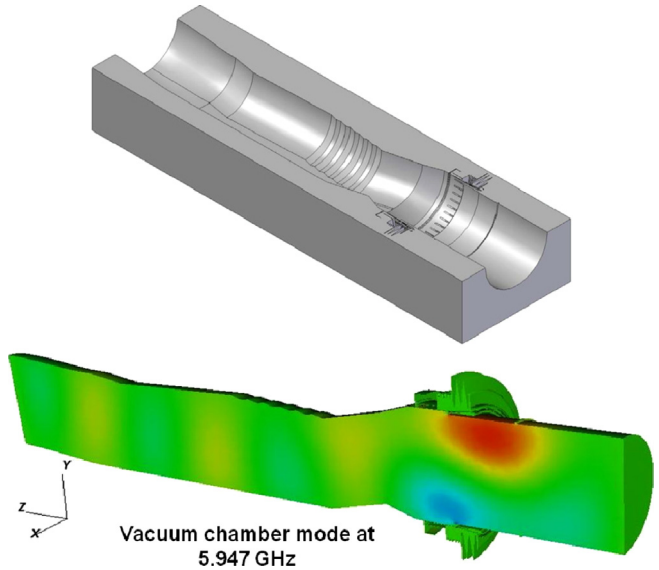

Fig. 6. Computer model of the interaction region. Red color correspond to a higher field; green color shows a smaller field, yellow is in the middle. (For interpretation of the references to color in this figure legend, the reader is referred to the web version of this article.)

3. Very thin gaps in RF seals

During the 2001 PEP-II run an unusual behavior of a valve body temperature [6] was observed in the low energy (positron) ring. The high positron current had elevated temperatures on different vacuum chamber elements like bellows and vacuum valves. The temperatures, measured by thermocouples, generally varied monotonically in accordance with the positron current. However, thermocouples placed on vacuum valve 2175 showed oscillations of temperature with a period of 3–8 min. The amplitude of the oscillations was of the order 5–20 F. The oscillations happened from time to time, when the positron current reached 1000 mA and more. A typical temperature oscillation is shown in Fig. 7. It was assumed that the gasket (RF gap ring), which is placed in the joint between the vacuum valve and the vacuum chamber, could have dimensions that are incorrect thereby producing a very small gap. We suspected that the gap size could be of order 100 μm. The positron beam through this size of a small gap could excite a cavity formed by the flange sides and the gaskets. Later we found traces of breakdowns (Fig. 7, right plot).

We did calculations of the loss factor of a simple model of a cavity and a small gap for different gap size and different beam radii. The left plot in Fig. 8 shows the loss factor.

It can be seen that the loss factor is almost constant but vanishes quickly at the gap size of 100–200 μm. However, the field in a gap goes up at smaller gap size (right plot at Fig.8). This can be the explanation of the mentioned above breakdowns. Simultaneously we found that several other valves had high temperatures. Fig. 9 shows photos of two valves destroyed by breakdowns of intensive HOMs excited in a valve cavity.

We have studied different models to understand how the temperature oscillations could occur. Here we discuss one model. A vacuum valve flange consists of two stainless steel parts, as it seen in right plot of Fig. 9. The parts are connected through a small circular Cu ring. Depending on the temperature difference, the

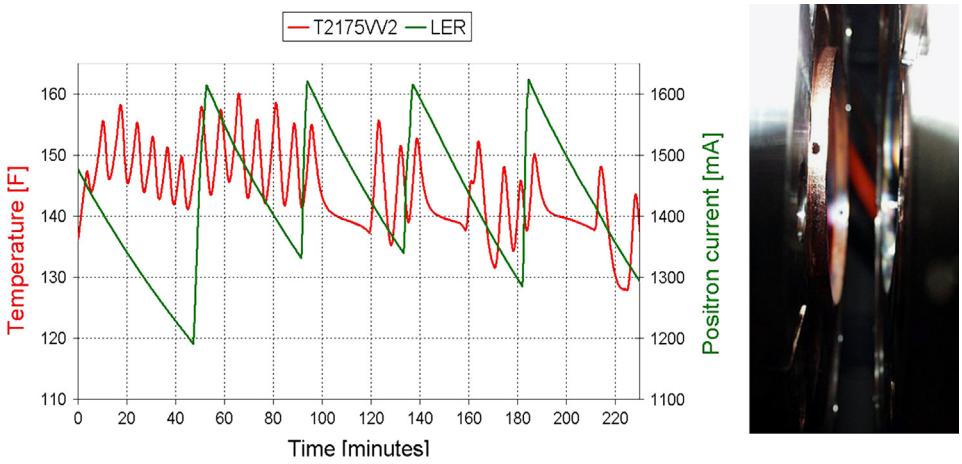

Fig. 7. Vacuum valve temperature (red) and positron current (green). Right photo shows traces of breakdowns. (For interpretation of the references to color in this figure legend, the reader is referred to the web version of this article.)

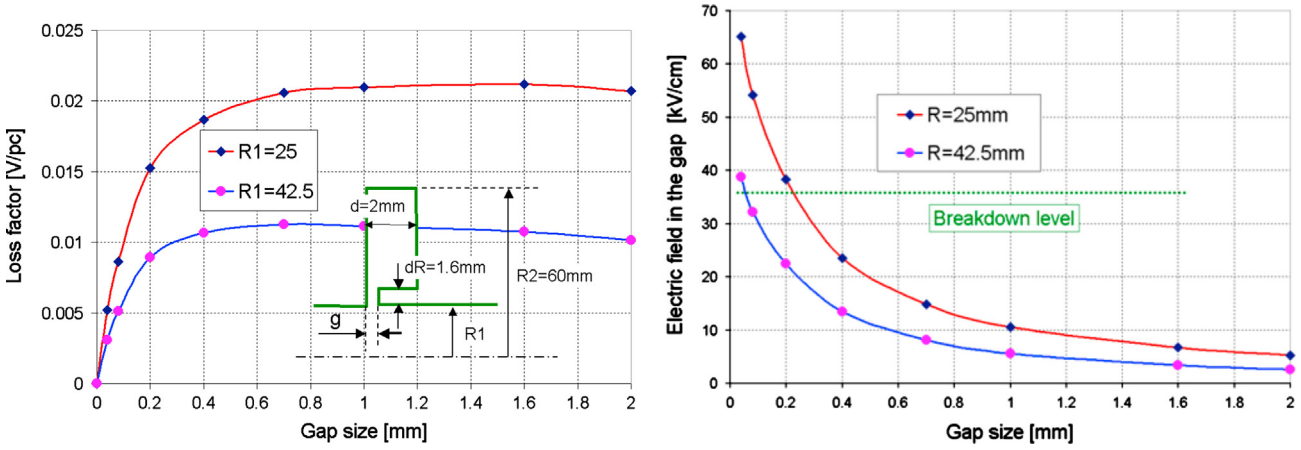

Fig. 8. Loss factor as a function of the gap size.

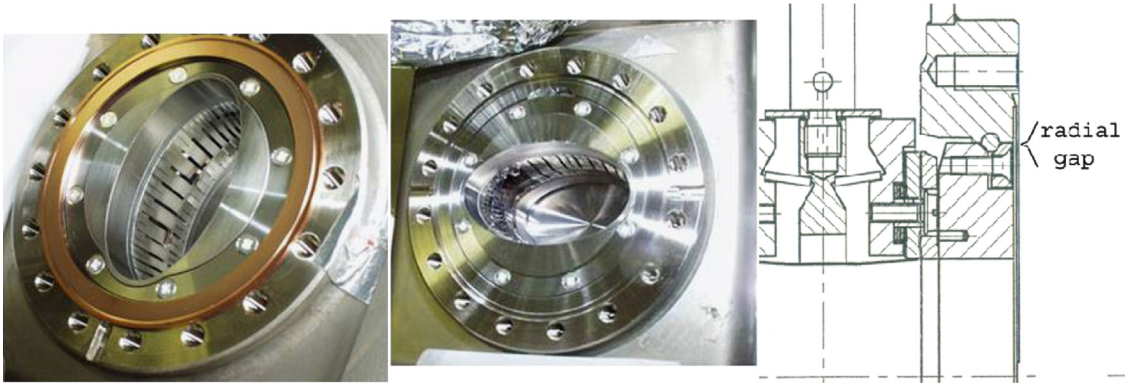

Fig. 9. Discharges in shielding fingers of vacuum valves and geometry of the valve flange. Note damaged fingers.

circular ring may not connect well with these parts and radial gaps could form on both sides of the ring. When the inner part of the flange is heated, as was discussed before, the size of these gaps decreases with the temperature and thermal contact is improved. The heat energy flows to the outer flange part, which was cooled with a fan and a Cu water-cooled disk. The temperature then goes down and the radial gap opens up once again. We developed a two-dimensional computer model to simulate this thermal effect. We found temperature oscillations, which are in good qualitative agreement with the experimental measurements.

Understanding the importance of small gaps in the beam pipe led us to a better design of the RF gap rings. After changing the gap rings we never saw the temperature oscillations return.

4. Gap ring, vacuum spikes and longitudinal instability

We had another experience with a gap ring that was installed incorrectly. At the end of 2005, the beam in the PEP-II Low Energy Ring became affected by an instability with a very fast growth rate,

but with a varying threshold [7]. Fig. 10 shows the statistics of aborts and X and Y position of the beam during the instability. The upper plot of Fig. 10 shows the beam loss starts with some delay (~100 turns) after beam excitation. Simultaneously we watched vacuum spikes in the region near one of the RF cavities (Fig. 11). The impression was that somewhere we had breakdowns, which disrupted the RF feedback system. We opened the vacuum chamber near this cavity and found a gap ring which had not been installed correctly. The right photo in Fig. 12 shows the gap ring, which has a cut in order to make it easier to install. The left photo shows how the ring was installed. One part of a sharp edge of the ring was inside the chamber as the middle part of the ring. These discontinuities in the chamber made it easy for trapped modes to be localized at this place. The sharp edges of the ring concentrate the electric field of the trapped modes and increase the probability of a discharge, when the beam current reaches some threshold. The electrical discharge produces vacuum spikes, which can be seen in the nearby ion pump. Also the beam particle dynamics may be affected by the vacuum spikes. Sometimes breakdowns can happen several times before the beam aborts,

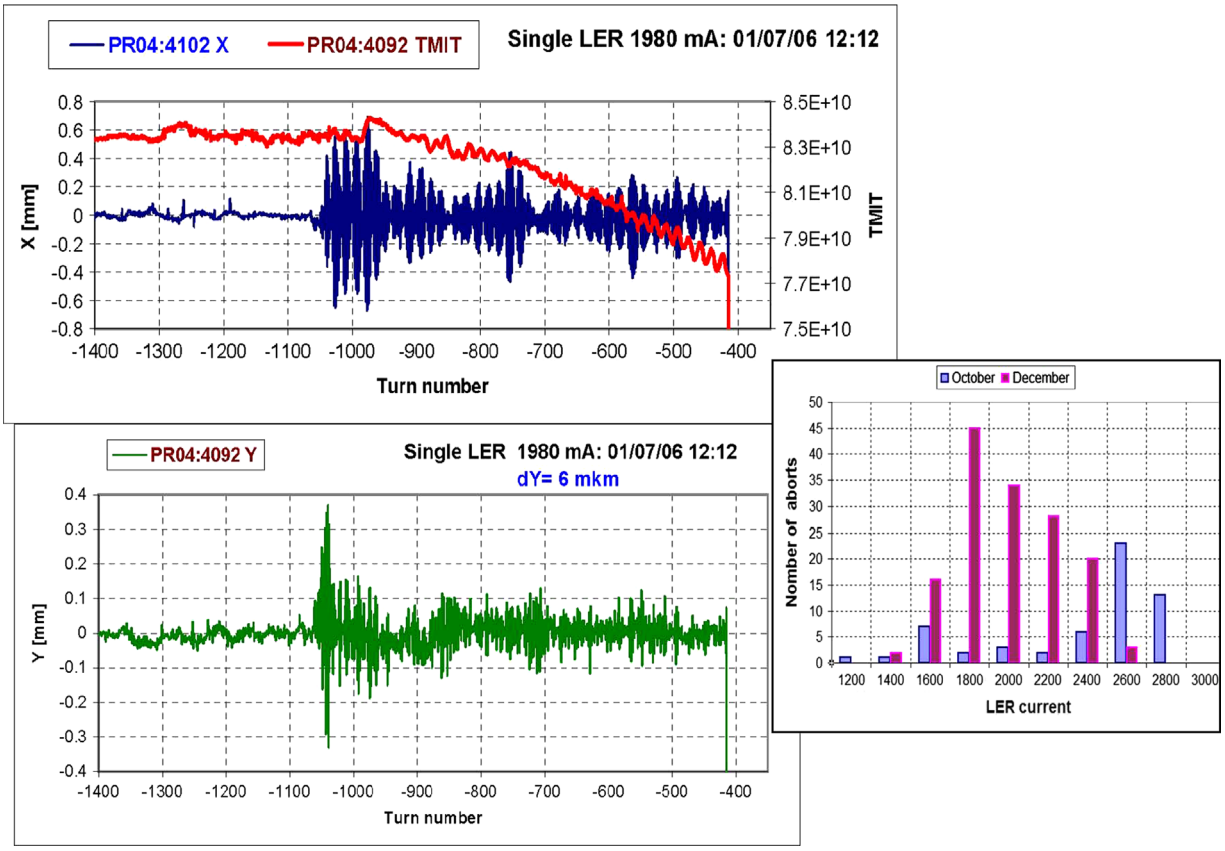

Fig. 10. X (blue) and Y (green) beam position during the fast instability. Red line shows bunch charge (TMT). Right plot shows statistics of aborts. (For interpretation of the references to color in this figure legend, the reader is referred to the web version of this article.)

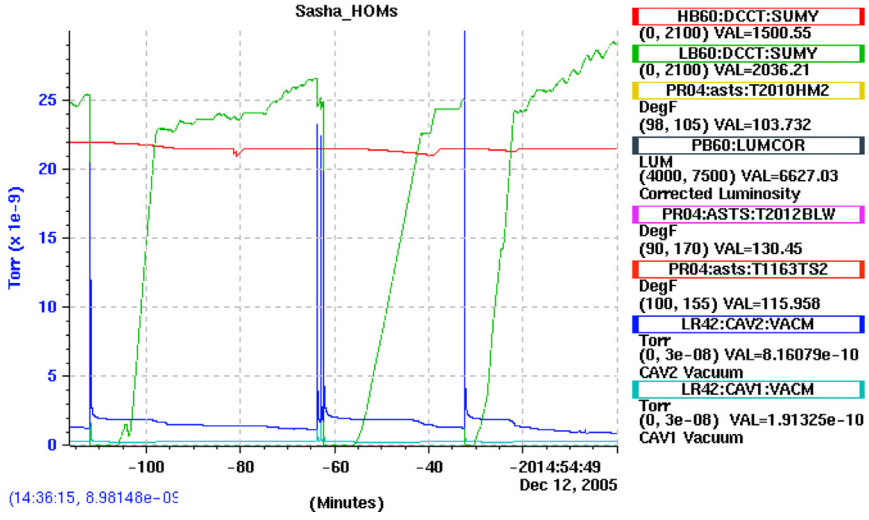

Fig. 11. Vacuum spikes (blue line) during each abort. Green line shows LER current. (For interpretation of the references to color in this figure legend, the reader is referred to the web version of this article.)

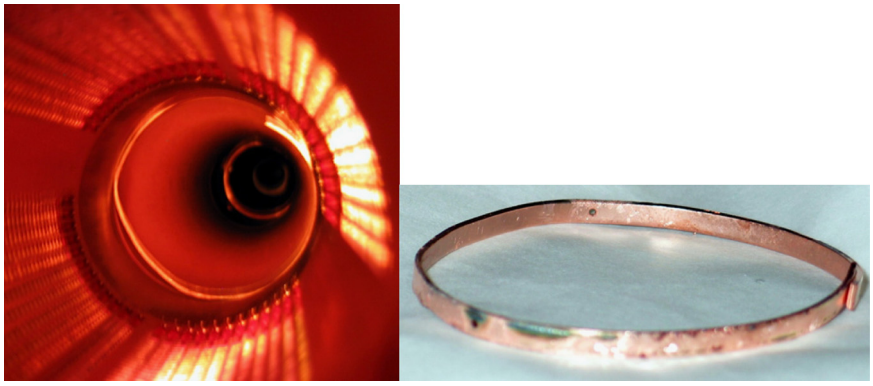

Fig. 12. Gap ring in the vacuum chamber and out.

as can be seen in Fig. 11. The discharge also transforms the stored energy of the trapped modes into a spectrum of high frequency waves which may freely propagate along the beam chamber and out through the BPMs and RF couplers in the cavities, which are used for RF feedback. Unexpected signals destroy the feedback system leading to particle loss and finally abort of the beam.

We solved the problem by properly installing a new gap ring. After that we no longer saw this kind of instability.

5. Resonances in HER shielded bellows

There was a very interesting effect we observed while monitoring the temperature of the HER bellows. Fig. 13 shows a typical example. While increasing the HER current, the temperature of some HER bellows would go up and then go down. We suggested this effect may be explained by an excitation of the resonance modes in the cavity behind the shielded fingers. Eigen-mode analyses using MAFIA code showed that several modes could be in resonance with bunch spacing frequencies. One of the modes is shown at the right plot in Fig. 14.

One side of a bellows is fixed, but other side is attached to a 5 m long Cu chamber. The long chamber absorbs the synchrotron radiation from the bend magnets. With increasing currents, the chamber temperature increases, the chamber length changes and the bellows section has to take this change. In this way, the bellows mode frequency may be changed and be in a resonance with the bunch spacing frequencies. We found later that these excitations happen when the bellows fingers are damaged (Fig. 14, left plot).

It is interesting that we have found one broken bellows in the high-energy ring by looking at the wake field signals from the low energy ring [8]. We designed a special device for watching wake fields in the low-energy ring near the interaction region (about 50 m from the IP). As we did not want to disturb the smoothness of the vacuum chamber, we used an existing vacuum port that had an RF screen, through which the HOM fields may be coupled to RF antenna. The screen was modified to allow more HOM power to leak through the screen. We had previously measured the spectrum of the HOMs using antennas, installed in the high voltage connections of a vacuum pump [9]. In that case, the HOM fields had to penetrate the RF screens and the pump itself in order to arrive at antenna. In this case, we decided to install a rod type RF antenna inside one arm of the pump cross to make it easier for the fields to go from the beam vacuum chamber to the antenna. In the arm, opposite to the antenna, we installed a water-cooled HOM absorber to capture and measure the HOM power. Thermocouples were attached to the supply and return water pipes to measure the

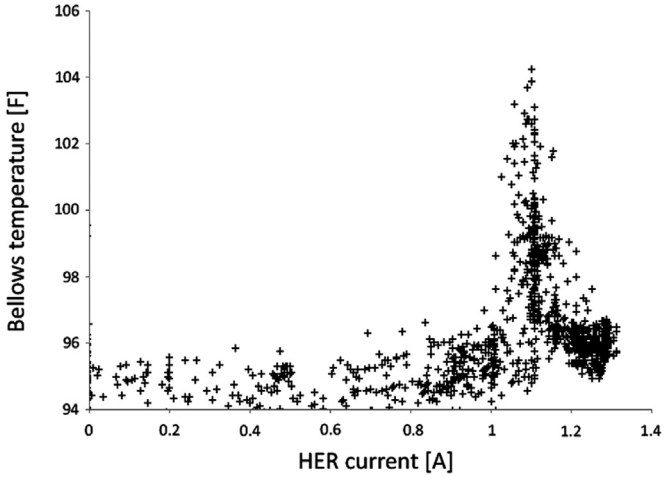

Fig. 13. HER bellows temperature as a function of HER current.

difference in water temperature. A photo of the pump cross with a pump, an antenna and a HOM absorber is shown in Fig. 15.

To increase the coupling between the beam vacuum chamber and the antenna we made longitudinal slots by connecting the holes in the RF screen (Fig. 15). Longitudinal slots allow only the transverse fields to couple to antenna. In this way, we did not increase the longitudinal impedance of the beam pipe. The cross pipe size is 35 mm in diameter, so the minimum frequency, which may be seen by antenna, is 4.8 GHz.

Watching an antenna signal in a single-bunch LER operation (upper plot of Fig.16) we see a signal coming from this location and a signal excited at the interaction region (IR). A positron bunch is coming from the interaction region to this location. Wake fields from IR are traveling with a group velocity, which is less than speed of light and gives some delay coming to the location of the antenna. Signal with a large delay may only come from beam chamber elements, located downstream of the antenna location.

We thought that the antenna might also see the wake fields excited by an electron (HER) bunch, because the separate LER and HER rings have a mutual 5-meter long vacuum chamber at the IR. Therefore, wake fields excited in one ring can propagate to another through the IR. In a single-bunch HER operation we expected to see the signal of the wake fields generated by the HER beam at IR. The signal should be approximately the same as what we see during single-bunch LER operation, but with a smaller amplitude as the bunch charge is smaller. However, what we actually saw was very different. The bottom plot of Fig. 16 shows this signal. There is a second large maximum or second signal with a delay to the first one of approximately 07–0.8 μs. The HER bunch travels

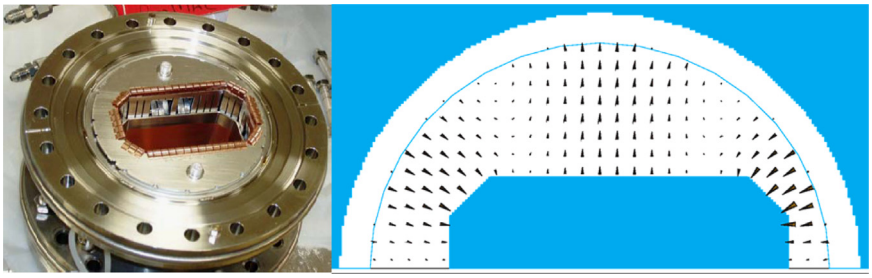

Fig. 14. Resonance mode in the cavity behind the bellows shielded fingers.

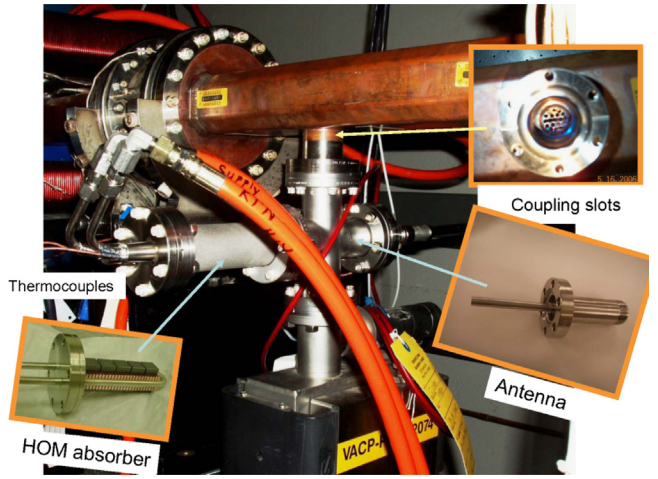

Fig. 15. LER ring. Pump cross with a rod type antenna and HOM absorber. Coupling slots in the RF screen filter the transverse fields.

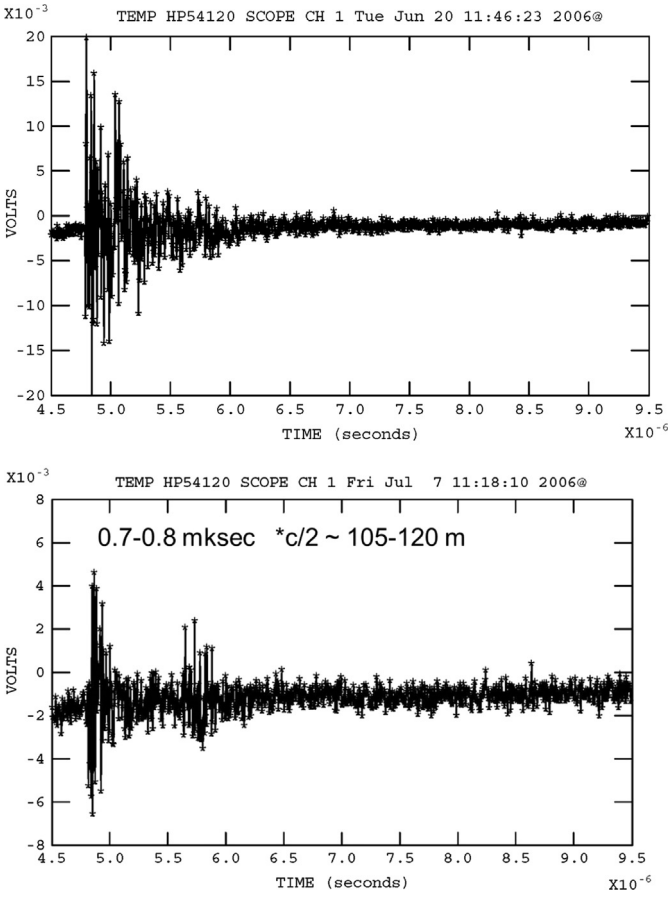

Fig. 16. Oscilloscope signal from the antenna in a single bunch LER operation (upper plot) and in a single bunch HER operation (lower plot).

away from the antenna at the IP so the delayed signal can be excited only after the HER bunch has passed IR. Fig. 17 shows the location of the antenna, IR and location, from which the delayed signal can come.

Using the time delay we estimated the distance between the interaction point (IP) and possible HOM source. The second (delayed) signal arrived at the antenna location after the first signal with a time delay equal to double the time needed for a bunch to travel from the IP to the HOM source location. The answer was about 105–120 m. At the time when we did this measurement, there was no indication of HOM heating in this region. Later when we increased the HER current and RF voltage, HOM heating became a problem in this region as well. We found a temperature rise at the "9062" bellows which is located around 100 m from IP, approximately at the same location, predicted by the antenna measurement. When we removed this bellows we found that it was completely broken. We may suggest that initially this bellows was not installed carefully. The reason for this can be the short length of the bellows fingers, which sometimes makes it difficult to install in tight locations. The deformed fingers produced a discontinuity of the smooth beam pipe and increased coupling to the bellows cavity. This led to the wake field excitation at this location, which we observed at the antenna. Later, with increasing currents and a shorter bunch length the stored energy in the resonant modes of the bellows cavity was enough to melt fingers due to arcs and electrical discharges. The photo of this bellows is shown at Fig. 18.

After the replacement of the bellows, we did another antenna measurement and found that the second signal had disappeared. The history plot of the temperatures in 9062-bellows showed that the HOM antenna found the damaged elements before it was uncovered due to the temperature elevation.

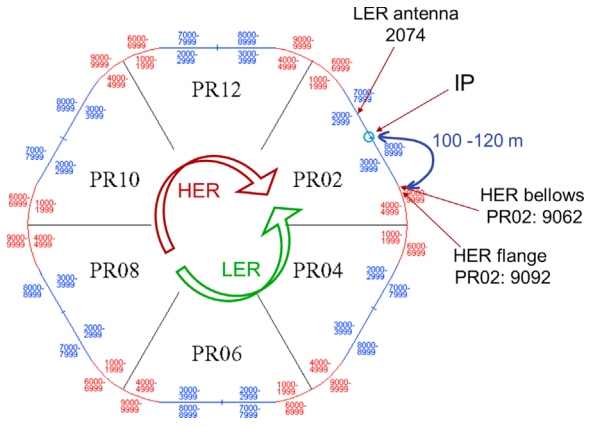

Fig. 17. PEP-II region map with position of LER antenna, interaction point (IP) and a HER bellows at the distance of 120 m from the IP.

6. "Fallen" BPMs

The HOM spectrum measured with the antenna is shown in Fig. 19. This spectrum was taken during a multi-bunch operation. The observed spectrum has a maximum at 7.38 GHz and smaller peaks in a 3 GHz frequency band. That confirms that HOMs generated in this region have significant power at the BPM resonant frequency. To monitor the beam position, hundreds of beam position monitors (BPMs) line the beam vacuum chamber. Each BPM consists of a round button electrode 15 mm in diameter which is mechanically press fitted to the 50 Ω feed-through connector.

While running at a shortened bunch length (9 mm at RF voltage of 4.5 MV) some of the upper button electrodes heated up enough to fall off their mounts at the LER current 2.4 A. The upper electrode fell onto the lower electrode as shown in Fig. 20 (left plot) which not only shorted the underlying electrode but also became a large obstacle for the beam fields, increasing the current though the lower electrode.

The origin of the heating is the wake field generated by an intense short bunch passing by the vacuum chamber discontinuity due to a through hole in a BPM button. The effect of beam fields on a PEP-II BPM are examined [10–11]. Scattering parameter analysis reveals resonant behavior near the frequency of 7 GHz. Time domain simulations show that maximum electric fields in the

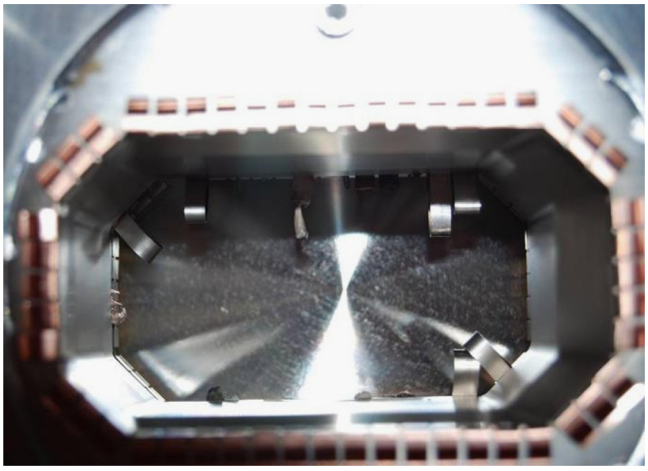

Fig. 18. Damaged and melted fingers of "9062" bellows.

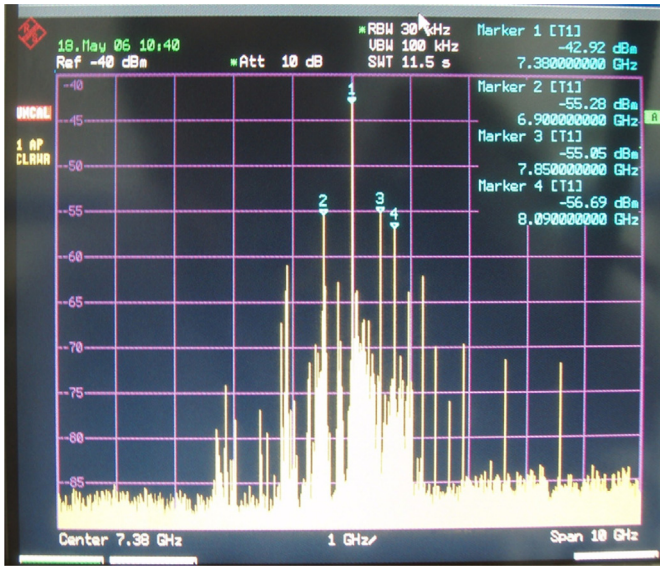

Fig. 19. HOM spectrum power [db] (not-calibrated), measured in a multi-bunch operation.

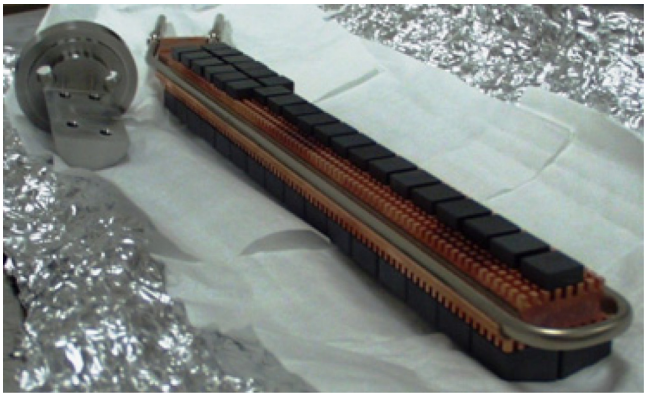

Fig. 21. Water-cooled HOM absorber.

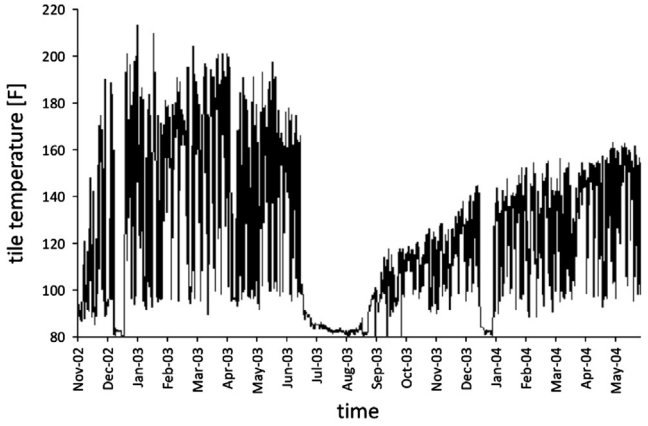

Fig. 22. Thermocouple readings (°F) before and after HOM absorber is installed.

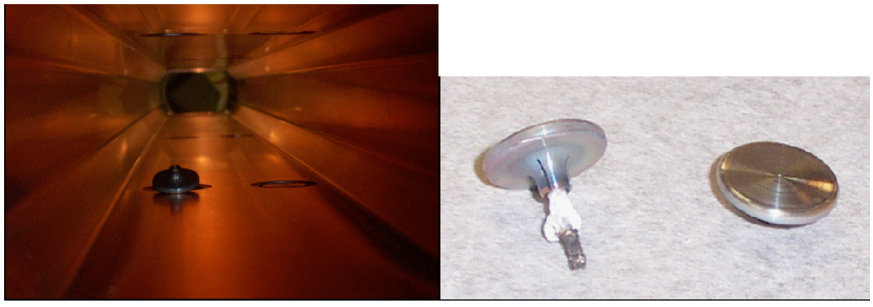

Fig. 20. A button of an upper BPM fell off onto a lower button (left plot). Melted feed-through of a lower button and the fallen upper button (right plot).

BPM are located at the up beam and down beam extremes of the BPM button corresponding to an excited dipole resonant mode in the BPM environment. At a resonant condition when a BPM mode is a harmonic of a bunch spacing frequency the fields of many bunches will be summed. Shorter bunches and higher currents will also raise the maximum electric field at the BPM, which can approach the breakdown voltage. As there is no cooling of the button, a small amount of power (10 W) is all that is needed to get the observed high temperatures up to near the melting point.

To remedy the situation, we invented a BPM puller that could be slid down the beam pipe, positioned under the BPM and then grab and pull the BPM button off of the pin in the ceramic feed-through. We initially thought we had lost the beam information from these BPMs but we were able to alter the electronics so that the signal coming from only the pins could be detected and used as beam position information.

7. Collimators and a burned feed-through cable

A temperature rise was found in the vacuum chamber elements in a junction of straight and arc chambers of the LER. The power in the wake fields was high enough to char beyond use the cable connector to the feed-through for the titanium sublimation pump (TSP) filament [12]. This pumping section is 5.5 m long and consists of the beam chamber and an ante-chamber. Electromagnetic fields, excited in the beam chamber penetrate to the ante-chamber and then through the filament feed-through of the TSP. To confirm that these electromagnetic fields were present a small ceramic tile with a high loss tangent was placed near the TSP feed-through on the cable just outside of the pumping chamber. A thermocouple attached to this tile showed a strong temperature rise. In order to study the spectrum of the fields, a short wire antenna was also placed there. The antenna was connected directly to a spectrum analyzer. Measurements show a wide frequency HOM spectrum with a maximum in the 2–3 GHz region. Based on these measurements a special water-cooled HOM absorber (Fig. 21) was designed and installed in the vacuum chamber.

As a result, the HOM power in the section decreased and the temperature rise went down. Thermocouple readings from the ceramic tile attached to the feed-though are shown in Fig. 22. The left side of the plot is the temperature before the HOM absorber was installed, and the right side shows the temperature after the HOM absorber installation. The temperature rise decreased by at least a factor of two even though the positron current increased by 40%.

The power loss in the absorber reached 1200 W for a positron beam current of 2.4 A.

The absorber helped us find the source of the HOMs. We did not find any significant correlations of the HOM power with the beam position in the vacuum chamber, but we found a strong correlation with the vertical beam position near vertical collimators, which are many meters away from this chamber. Fig. 23 shows the HOM power in the absorber (red line) and the vertical beam position near the collimator that is 15 m away (blue line) and the collimator that is 65 m away (green line). It can be seen that a 10 mm vertical change in beam orbit at the closer collimator reduced the HOM power almost two times. The same (~10 mm) change of the beam position in the 65 m collimator changed the power in the absorber by an additional 10%.

We observed almost the same power change in the arc bellows. This bellows also takes HOM power from the horizontal collimators (Fig. 24).

Measurements indicate that the HOM power is almost linear with the RF voltage (Fig. 25) and inversely proportional to the number of bunches. These relations give the following approximation for the HOM power P

$$P_{[W]} = 0.07 \times I^2_{[A]} \times \frac{V_{RF[V]}}{N_{\text{bunches}}}$$

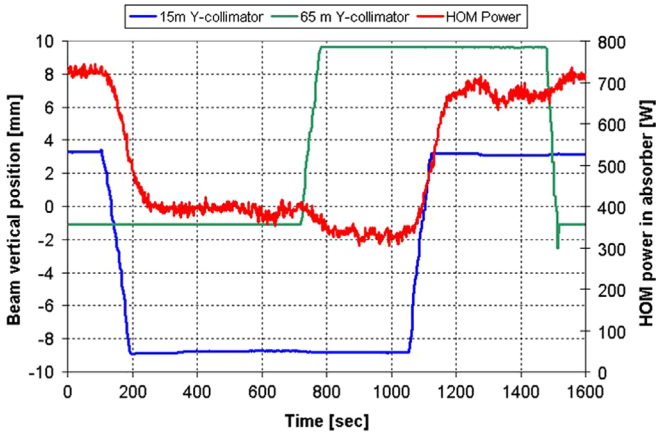

Fig. 23. HOM power in the absorber (red line) and the vertical beam position at the 15 m collimator (blue line) and 65 m collimator (green line). (For interpretation of the references to color in this figure legend, the reader is referred to the web version of this article.)

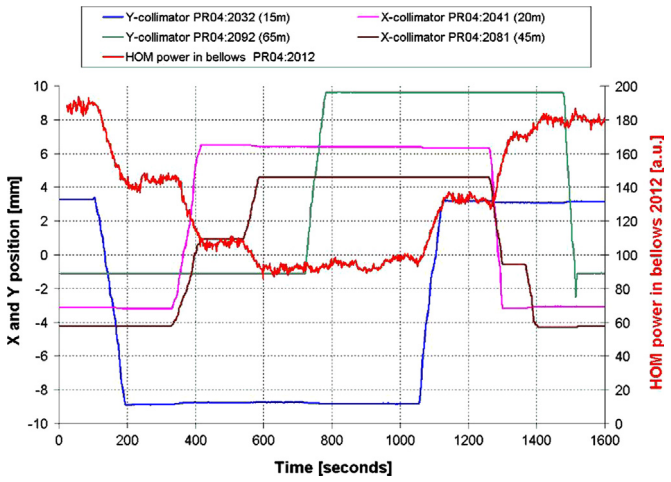

Fig. 24. HOM power (red line) in the arc bellows and beam position near vertical (blue and green lines) and horizontal collimators (pink and brown lines). (For interpretation of the references to color in this figure legend, the reader is referred to the web version of this article.)

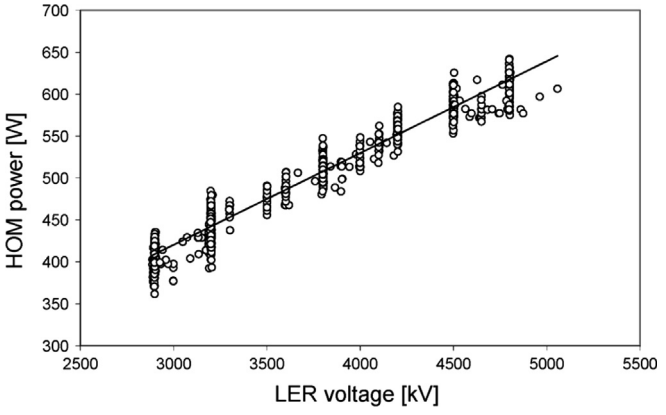

Fig. 25. HOM power vs. RF voltage for a positron current of 1400 mA.

were I is the positron beam current, N_{bunches} is the number of positron bunches and V_{RF} is the RF voltage.

We performed wake field simulations and results showed very good agreement with these measurements. In the simulation we found that the beams at a collimator produce mainly dipole and quadrupole transverse fields (Fig. 26).

At the beginning, the wake fields have a quadrupole structure, but later the dipole mode becomes the main component of the field. These fields can propagate long distances and penetrate through the shielded fingers into bellows and vacuum valve cavities.

The calculated loss factor, presented in Fig. 27 confirms that beams excite more fields when they approach the vertical collimator in the vertical direction, whereas a horizontal displacement does not strongly change the HOM power. Simulations also confirm the quadratic dependence of the HOM power upon the bunch length in the range of 8–13 mm.

We developed a new water-cooled absorber (Fig. 28) to capture the wake fields generated from collimators [13]. The absorbing ceramic tiles couple strongly to transverse fields through long,

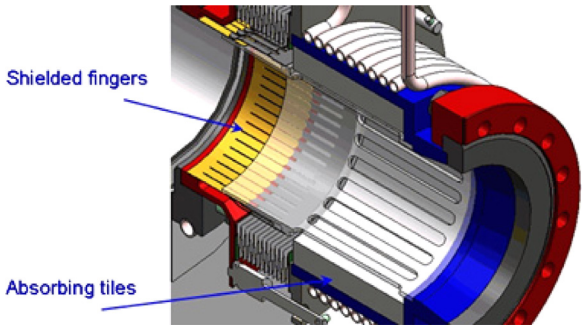

Fig. 28. Straight section HOM absorber.

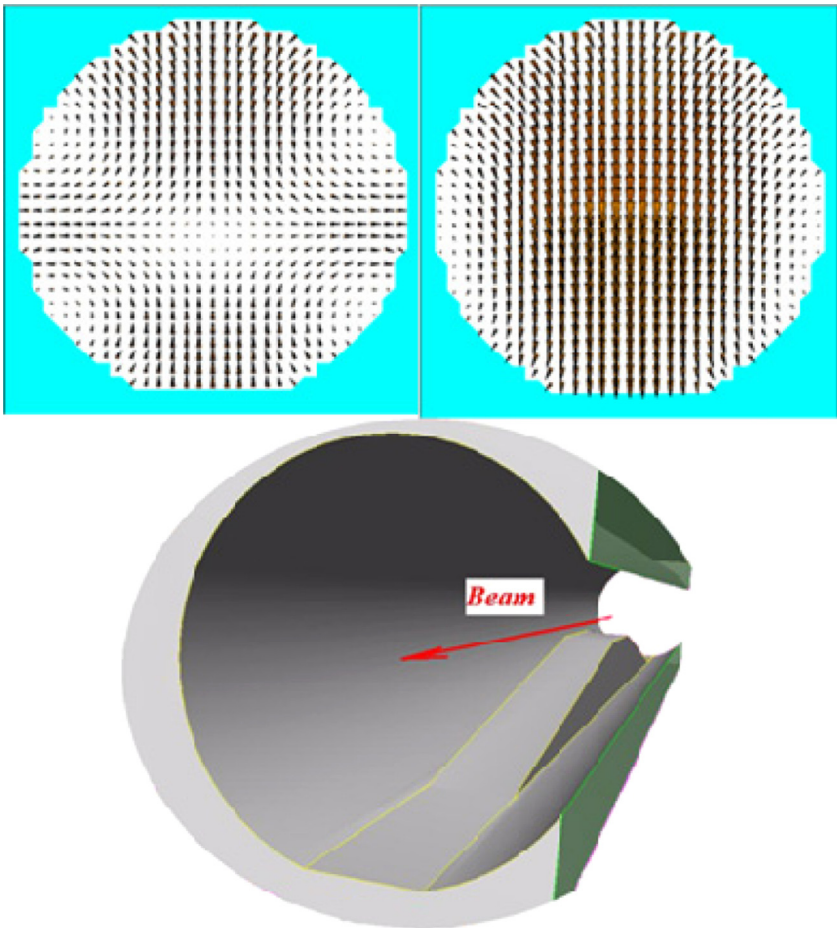

Fig. 26. Beams near collimator generate dipole and quadrupole transverse fields.

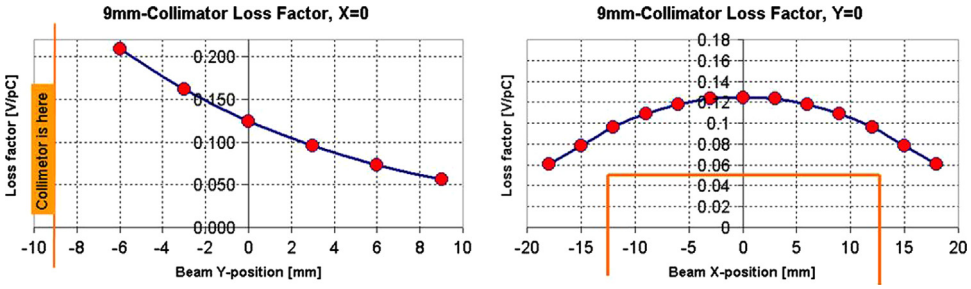

Fig. 27. Loss factor as a function of a Y and X beam position.

wide longitudinal slots, whereas the longitudinal field can freely propagate through the chamber.

We installed this kind of absorber after each collimator (Fig. 29).

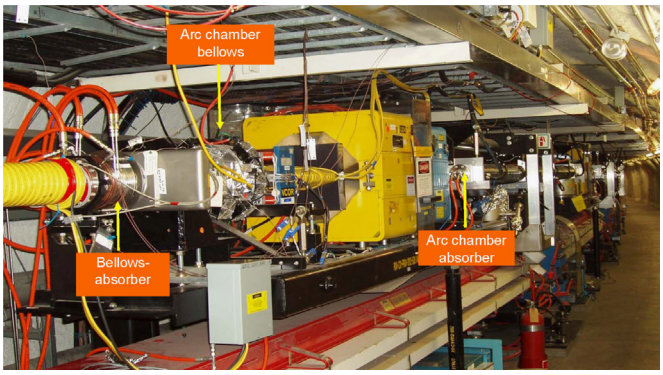

Fig. 29. HOM bellows-absorber in PEP-II.

8. Melting omega seals

At the level of 1.7–1.8 A in the HER we encountered a stochastically distributed series of vacuum bursts almost everywhere in the arcs [14–15]. Thermocouples attached to flanges also showed random temperature rises and oscillations. RF omega seals installed between these flange joints were designed to keep the inside of the beam pipe RF smooth. This flex joint moves in order to compensate for beam pipe motion due to synchrotron radiation heating in the 5.4 m bend magnets. Unfortunately, we found that the flexibility was not adequate at the higher HER beam current leading to partially crushed seals. This let RF power leak into the volume behind these seals. As a result, nearly every one of the omega seals was damaged and partially melted (Fig. 30).

At first, as shown in the plot, the temperature is linear with the current, since the synchrotron radiation heating is proportional to the current. Then at some current, the temperature jumps up. This suggests that at some current, or more precisely at some chamber temperature, a gap appears in the beam pipe joints and the beam starts generating wake fields. These fields go into the gap and heat the stainless steel disk, which supports the omega seal. If the gap environment has a high Q-value for RF modes, then the heating

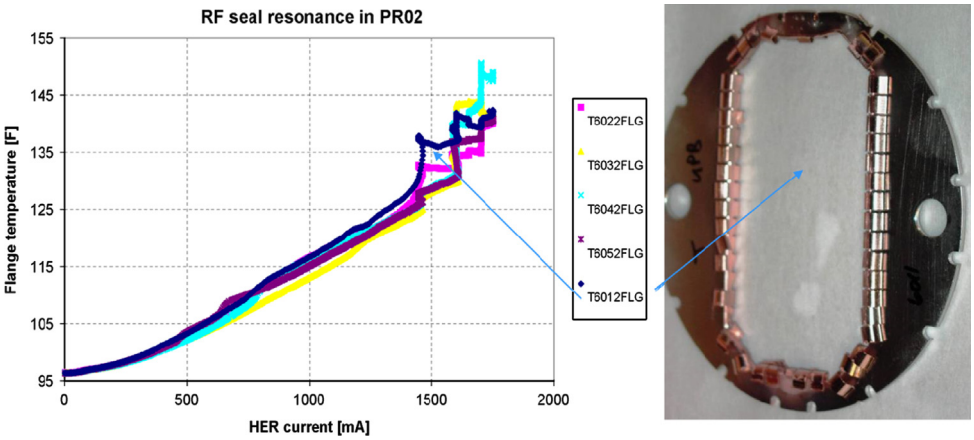

Fig. 30. HER temperature resonances and omega seal. The left plot shows the typical behavior of the flange temperatures with the HER current. Here we present temperatures of five consecutive flanges in the Arc 1.

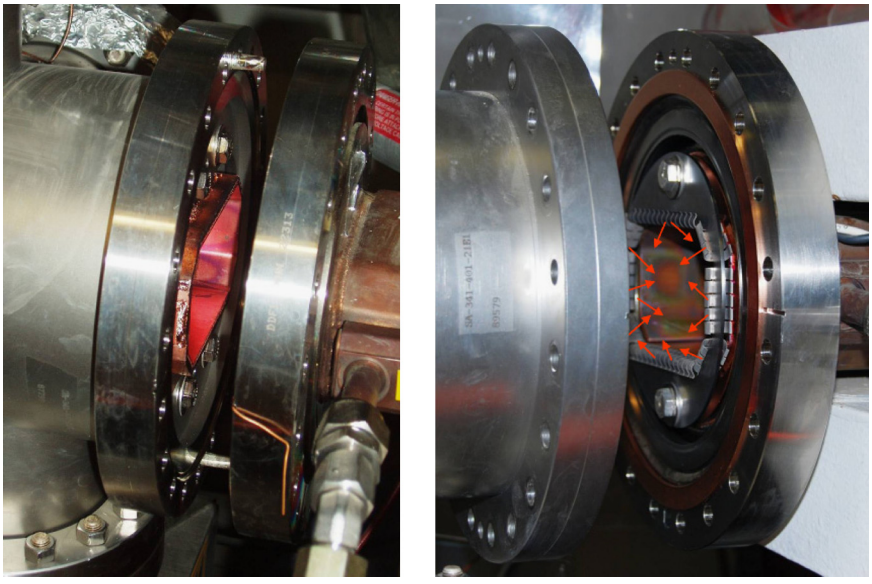

Fig. 31. HER flanges and flexible omega seal. Red arrows show the how the seal may be cooled by thermal radiation. (For interpretation of the references to color in this figure legend, the reader is referred to the web version of this article.)

may be much stronger. As there is no special water-cooling, the disk temperature can go very high and be limited only by thermal radiation. Resonance temperature behavior can be explained by the coupling through the gap and the existence of high Q-value RF modes.

On investigation, we found out that the space behind the omega seal has a fairly large volume. Fig. 30 shows neighboring flanges and an omega seal with its support stainless steel disk. Some Cu parts of the flanges where the seal touched the surface show traces of breakdown (left photo in Fig. 31). The left beam pipe branches out from the flange disk, making a sort of coaxial RF cavity. If an omega seal starts to open a gap, then the open gap starts to behave like a capacitor of a quarter-wave cavity. Let us define the volume outside the seal as a "sealed cavity".

To make a quick estimation of the fields inside this sealed cavity we made a simple 2-d model, which is shown in Fig. 32.

In this model, an omega seal loses contact with the flange on both sides. We assume both open gaps have the same size. We made analyses using the code "NOVO" [16]. A bunch, moving in the beam pipe excites electromagnetic fields in the cavity through these gaps. The blue lines show the electric force lines of the excited field. The absorbed power P in the sealed cavity may be calculated according to the formula

$$p = \tfrac{1}{2} K \tau_b I^2.$$

We assume that half of the power goes inside the sealed cavity and half of the power travels in the beam pipe. The beam current $I = 1.8$ A, the bunch spacing $\tau_b = 4.2$ ns. The loss factor K is a function of the gap size and varies from 0.01 V/pC to 0.07 V/pC for the gaps of 0.1–1.0 mm. We had an 11 mm bunch in the HER at RF voltage of 16.5 MV. The absorbed power in the sealed cavity at a gap size of 0.05 mm is approximately 60 W. The electric field increases with the smaller gap size and reaches a breakdown limit

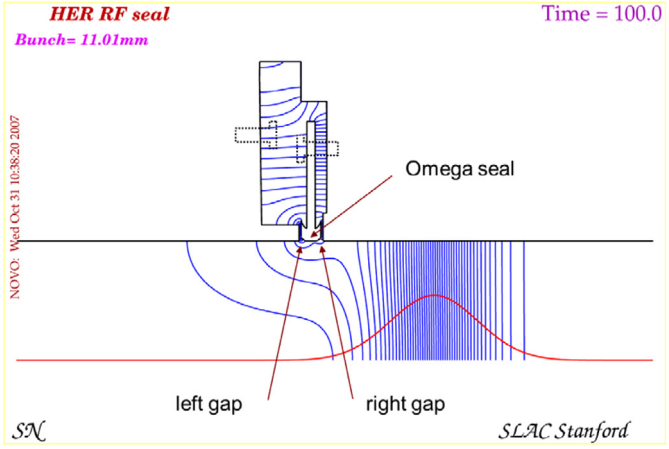

Fig. 32. Computer model HER flanges forming a sealed cavity and a flexible omega seal.

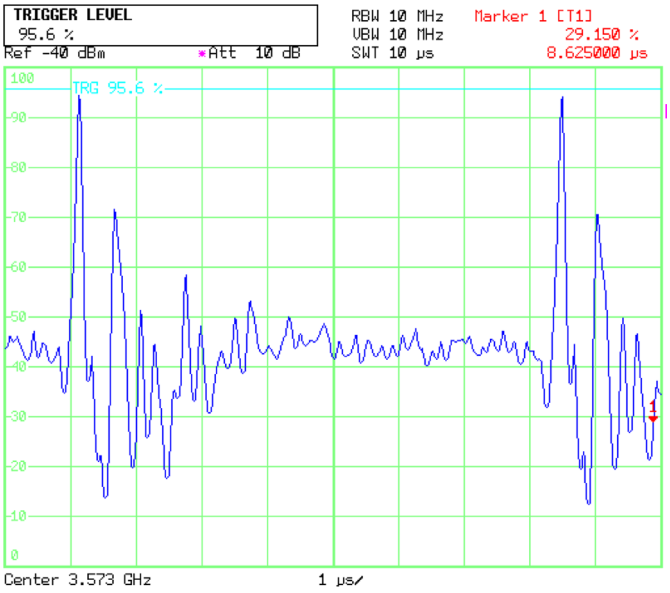

Fig. 33. Transient signal [db] (not-calibrated) at frequency 3.8 GHz.

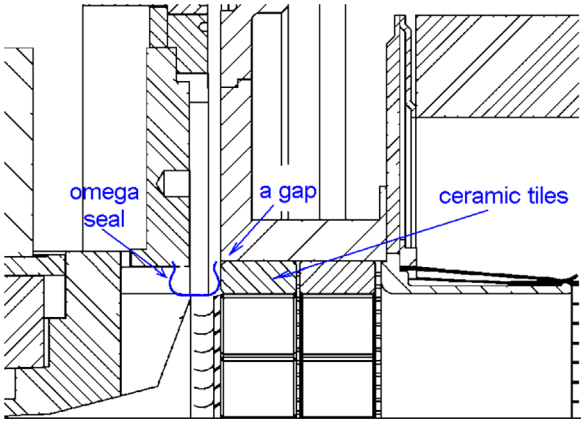

Fig. 34. Layout of Q2-bellows (one half), which includes ceramic tiles and omega seal.

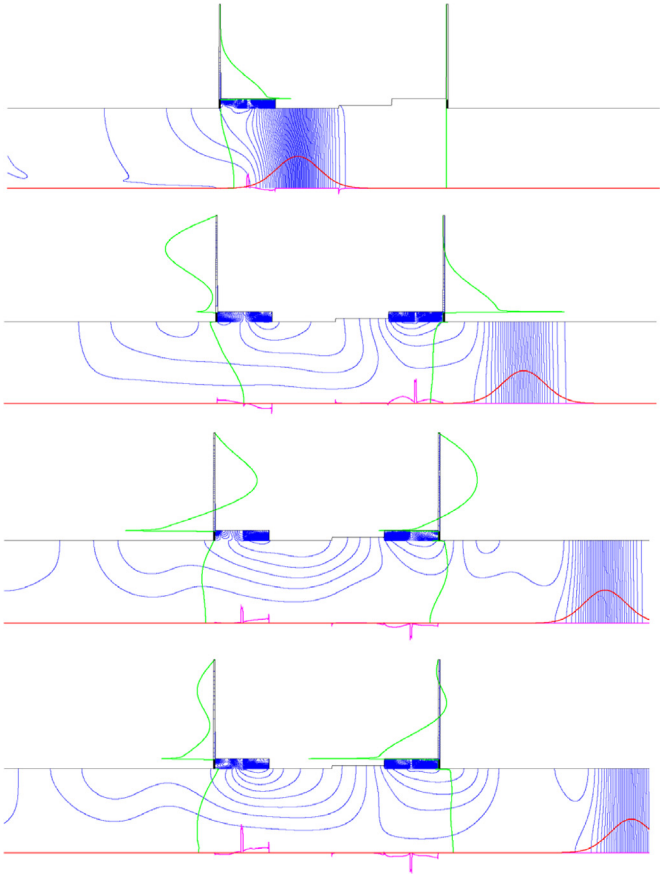

Fig. 35. Snapshots of the electric displacement force lines at different times during a bunch passage. (For interpretation of the references to color in this figure legend, the reader is referred to the web version of this article.)

(we assume 30 kV/cm) when the gap size is less than 0.05 mm for a HER current of 1.8 A. These results show that breakdowns may happen in a gap, what is seen at Fig. 30. The stainless steel disk that supports the omega seal absorbs power that comes into the cavity. Its temperature increases until thermal radiation between the seal and the beam pipe start to work. We can estimate this power using the Stefan–Boltzmann law for black body emissive radiation:

$$P_{BB} = A\varepsilon\sigma T^4 \quad \sigma = \frac{2\pi^5 K^4}{15c^2h^3} = 5.67 \times 10^{-8}\frac{W}{m^2K^4}$$

We assume that temperature T is of order of the melting point of Cu (1350 K). The area is the surface of the seal facing the beam chamber and we assume an emissivity of 0.2. For these parameters, the thermal emission power is 55 W, which is very close to the power absorbed in the sealed cavity. Naturally, at this high temperature, there can be other ways for the radiation power to escape, for example, through stainless steel flanges. These effects will increase the power needed to reach the melting temperature. However, breakdowns and arcing in the gap will localize the power in the omega seal. Several seals were found where parts of the stainless steel disk had melted indicating the temperature had risen up to at least 1400 K.

The left flange of Fig. 31 has two holes, which connects the gap environment to a vacuum pump. The fields excited in the gap may propagate to the pump through these holes. We attached an antenna to the high voltage pump connector to study the spectrum of these fields. The spectrum showed a large peak at 3.8 GHz in a multi-bunch operation. We did a transient measurement during a time gap between bunch trains at this frequency. The measured signal is shown in Fig. 33. One can see that the damping time of this mode is at least 0.5 μs, which means that this mode has a high Q-value of 1900.

An Inconel alloy was used to replace GlidCop omega seals. This material has a much better spring constant and is less prone to crushing as well as having more resistance to high temperatures. We also silver-plated the omega seal and stainless support disk assembly in order to produce a high conductivity surface and reduce the power absorption in the stainless steel.

9. Beam fields on ceramics

In 2005 PEP-II achieved a peak luminosity of 10^{34} cm^{-2} s^{-1} with beam currents of 2.94 A in the LER and 1.74 A in the HER just before shutting down for a month. Upon starting up again, we discovered we were unable to sustain LER currents much above 2 A without an abort occurring due to high radiation levels in the detector. The problem was the occurrence of very fast, very high pressure spikes in the vacuum chamber just upstream of the detector. The radiation levels in the detector caused by these gas events were too high and the beam had to be aborted [17–18]. This problem quickly became chronic.

Several attempts were made to push through this limit with no success. A wide variety of experiments was conducted to isolate the source of the problem or eliminate possible causes. The HOM tiles located in the Q2-bellows had always been considered suspect. These Q2-bellows were situated at a distance of 2.2 m from IP. This bellows is the last shared vacuum element before the beams enter separate chambers. The ceramic tiles absorb HOM power of over 10 kW. Among the possibilities we considered was that the tiles got very hot and perhaps outgassed because of breakdowns due to the high electric fields initiated by the high LER and HER currents. In addition, to the geometrical wake (because of the very complicated geometry of the interaction region) the Q2-bellows also produces Cherenkov radiation. The reason for this is the high permittivity of the tiles. The ceramic tiles are open to the beam, so they capture and store some part of the beam field and then these fields are radiated.

After we checked the bellows drawings and an intonnel inspection it became clear that the omega seal that is next to the tiles had been designed incorrectly. The metal spring fingers of these seals were touching the tiles (which are insulators) instead of touching the metal surface under the tiles. Any sharp edge of a

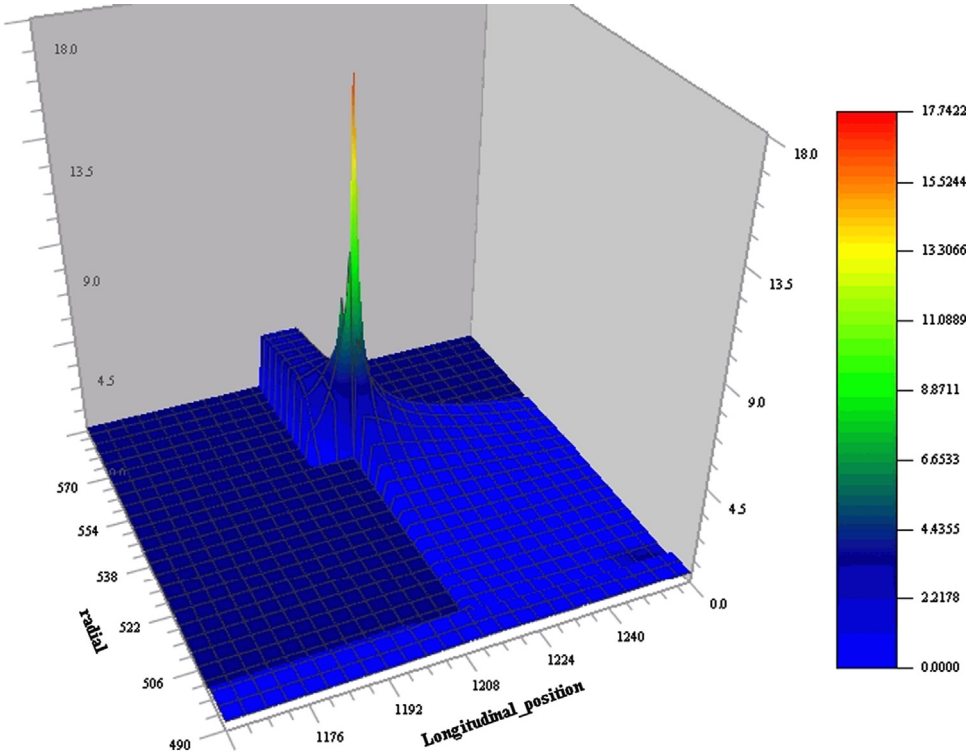

Fig. 36. Electric field distribution in the region between an omega seal and ceramic tiles.

seal finger, which is very close to a ceramic tile may strengthen the electric field many times causing sparking or breakdowns. Then very fast high-pressure spikes can be easily explained by these stochastic breakdowns. To study this possibility we carried out computer simulations of the excitation of the electromagnetic fields in the ceramic tiles by the fields of circulating LER and HER bunches. In the model we assumed that the effect has more bunch charge dependence than total current dependence, and a higher current LER beam produces consistently higher fields and consequently higher radiation levels than the HER beam. The layout of the Q2-bellows in a vacuum chamber is illustrated in Fig. 34. If an omega seal touches a ceramic tile only, then a small gap opens up and the electromagnetic field can propagate inside the gap between two flanges. A sharp edge of the seal will concentrate the electric field, which will also be large at a ceramic edge. If the electric field is above the breakdown threshold, then a surface arc can develop on the tile and ceramic atoms will explode with a burst of ions appearing in the vacuum system. Once a surface track has been established the beam current threshold for producing another surface arc was lowered from 2.9 A to less than 2 A. The tile material contained AlN+40% SiC. RGA studies of the vacuum bursts had indicated the presence of nitrogen.

The geometry of the simulation model and snapshots of the electric field force lines at different times are shown in Fig. 35. The black box approximates the omega seal, the ceramic tiles are shown as a concentration of electromagnetic fields (blue lines). The red curve shows the bunch shape. The green curve shows the electric field distribution along the transverse plane that touches one side of the gap. The pink curve shows the electric field along the surface of the vacuum chamber and ceramic tiles. Bellows fingers are approximated as a step in the vacuum chamber.

Strong fields at the sharp corners of the omega spring and in the gaps between tiles are induced several times during the passage of the bunch. The direction of these fields is also changing in time, so they may produce current emission from a metal surface or from the tile surface. The time duration of the fields in ceramic tiles depends upon the permittivity and dielectric losses, which are in our case are $\varepsilon=30$ and $\tan\delta=0.1$ We can estimate this time for a tile thickness d by the formula [19]

$$T_{\text{tile}} = 4\frac{d}{c}\frac{\sqrt{\varepsilon}}{\tan\delta}$$

For $d=4$ mm the formula gives a field duration of $T_{\text{tile}} = 2.9$ ns This time is less than the time distance between two LER bunches (4.2 ns), but is larger than the time between the arrival of the LER and HER bunches (2 ns). So the field induced by a LER bunch can be strengthened by a HER bunch. However, fields in a cavity between stainless steel and Cu flanges may survive for a much longer time. We may estimate the filling time of the order of 20 ns, which means the fields in a cavity will increase 8 times (including HER bunches).To find critical points we studied the electric field distribution at different parts of the Q2-bellows. In this simulation, the gap between the omega seal and the metal part was 0.5 mm and the bunch length was 13 mm. Fig. 36 shows the most critical point: the omega seal corner near a ceramic tile. Calculation resulted in a maximum value for electric field of 17.7 V/m/pC.

If we assume that the field may stay in the cavity between the flanges for 20 ns, then the peak electric field can reach 40 kV/cm comparable to the breakdown limit for the ceramic material. Upon opening the beam chamber, we found electrical burn marks and lost material in two ceramic tiles (Fig. 37). A close look shows a small discoloration on the edge of the top row of tiles. The breakdown appears to start at the corner of the tile and then travel along the surface of the tile to the Cu underneath the tile. The damaged tile is a little closer to the LER than to the HER. The omega seal that mated with the damaged tile has melted Cu edges.

10. IP wake fields and a new Q2-bellows

PEP-II IP region has a very complicated structure due to the conjunction of LER and HER beam pipes and various types of synchrotron radiation masks. Calculations and measurement showed that for a bunch length of 6–14 mm, the loss factor is an

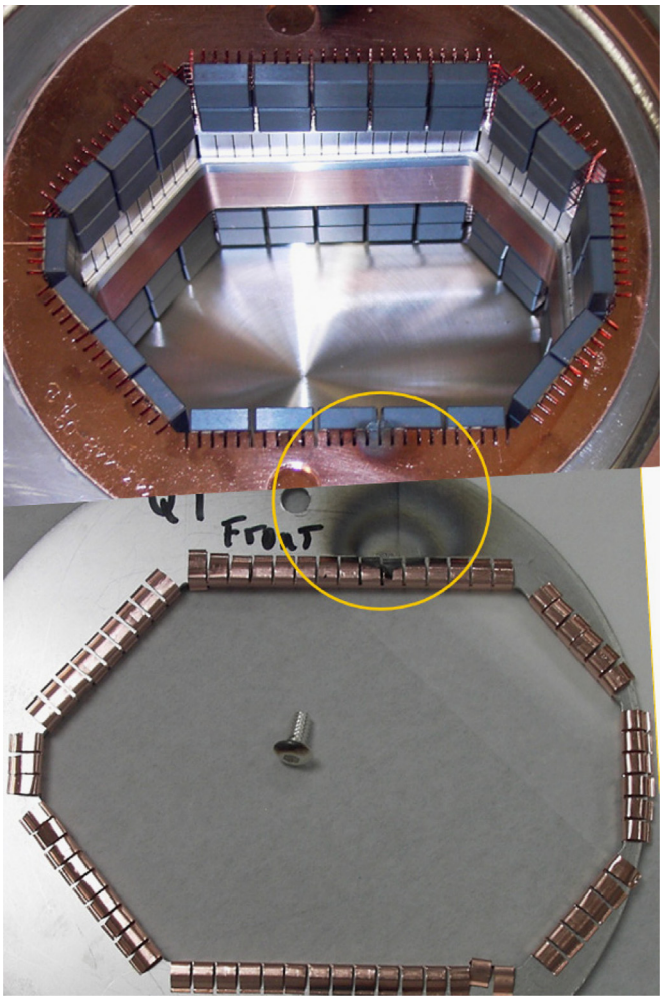

Fig. 37. Q2-bellows and Ω-seal with traces of sparking.

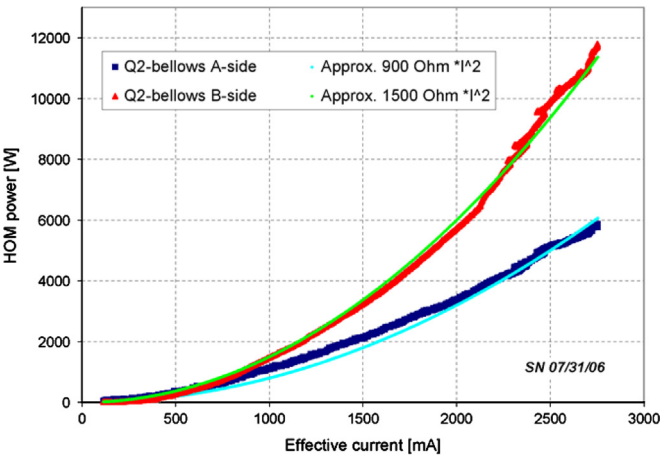

Fig. 38. HOM power in the Q2-bellows. LER RF voltage is 4.05 MV, HER RF voltage is 15.4 MV, number of bunches is 1722. (For interpretation of the references to color in this figure legend, the reader is referred to the web version of this article.)

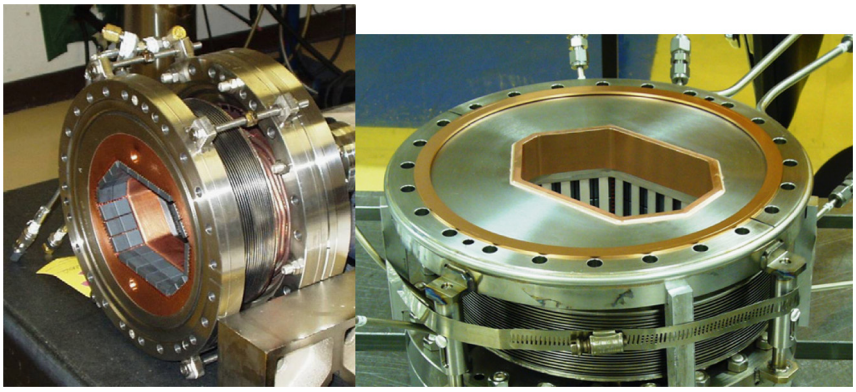

Fig. 39. Old (left) and new (right) Q2-bellows absorbers.

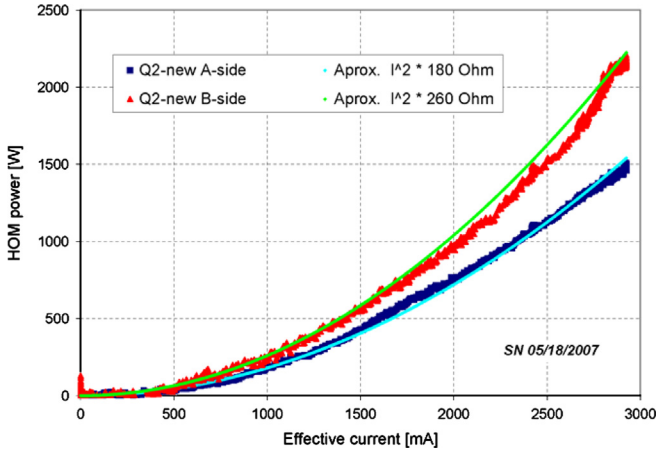

Fig. 40. HOM power in all new Q2-bellows.

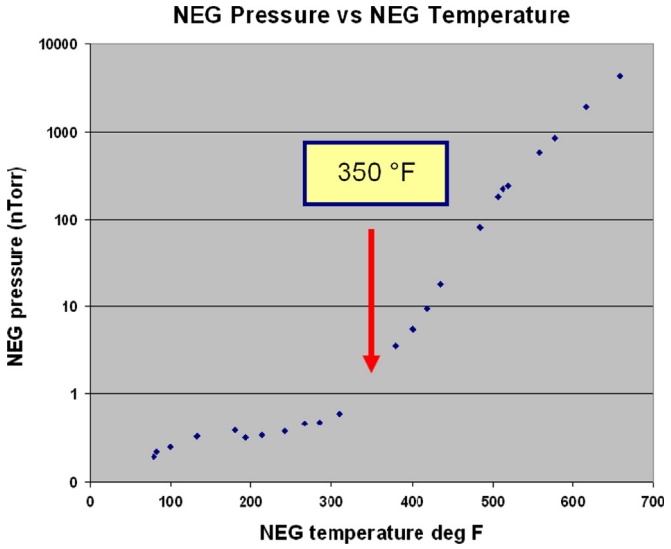

Fig. 41. Plot of a NEG pressure as a function of NEG temperature. At about 350 °F (180 °C) the NEG starts to outgas.

inverse quadratic function of the bunch length or linear with RF voltage. For shorter bunches (1–6 mm) the quadratic dependence changes to the exponent to 3/2. If we assume that fields generated by the LER beam are not coherent with fields generated by the HER beam, then the effective current is determined by the formula:

$$I_{\mathrm{eff}} = \sqrt{I^2{}_{\mathrm{LER}} + I^2{}_{\mathrm{HER}}}$$

To estimate the Cherenkov radiation power we use formulas which were derived for a "thick" dielectric tube of radius a and length L [19]. In the case of a bunch length σ larger than the effective dielectric wavelength $s = a\sqrt{\varepsilon - 1}/2\varepsilon$, the loss factor is described by the formula.

$$k = \frac{cZ_0 L}{2\pi a^2} \times \frac{s}{\sqrt{\pi\sigma}} \approx \frac{cZ_0}{4\pi^{3/2} a} \times \frac{L}{\sigma\sqrt{\varepsilon}}$$

where the Z_0 is the free space impedance and c is the speed of light.

The dielectric constant of ceramic tiles is high ($\varepsilon = 22$) even at higher frequencies (8 GHz). For a beam radius of 50 mm the mentioned condition works well for a bunch length of 13 mm and the additional radiation loss factor is estimated to be 0.187 V/pC for the total tile length of 112 mm. This number is comparable with a geometric loss factor 0.248 V/pC. That means we almost double the HOM power at the IP only because the ceramic tiles are exposed to the beam. The total IP HOM power is of order of 20 kW for a bunch spacing of 4.2 ns. We compare this number with results of experimental measurement. To measure the HOM power dissipated in the Q2-bellows we used thermocouples installed at the supply and return water-cooling channels. We also measure the water flow. The HOM power as a function of the effective current is shown in Fig. 38. The quadratic approximation (green and light blue lines) is also shown. The absorbing power reached 12 kW on the right side of the IP and 6 KW on the left side.

A simple solution to cancel Cherenkov radiation is to isolate the ceramic tiles from the beam by a metal sleeve with longitudinal slots. We determined the required slot length by keeping the same absorption for the dipole and quadrupole modes. We designed a new Q2-bellows based on the wake field simulations [20]. The photo of the old and new absorber is shown in Fig. 39.

Results of the power measurements with new Q2-absorbers are shown at Fig. 40. The amount of absorbed power changed dramatically. We had been producing a lot of wake field power due to the ceramic tiles being open to the beam. It is very important to note that we did not observe any dramatic temperature change in the vertex bellows, which are situated between the Q2-bellows. This means the Q2-bellows absorb transverse fields well, and do not allow them to propagate to the inside section of the IP region.

11. Loss factors of the rings

We also developed a method to measure loss factor of the rings using data from the RF feedback system [21]. These measurements

showed that the loss factor of LER is on average 6 V/pC, and the loss factor of the HER is several times higher at 22 V/pC [22]. Wake field calculations produce good agreement for the LER, but cannot fully explain high loss factor that was seen in the HER [23].

12. NEG vacuum pump heating

A great deal of effort was made to minimize the vacuum pressure upstream of the interaction region for both beams. Special Non-Evaporable Getter (NEG) pump constructions were used and these pumps were placed in side chambers of the beam pipe with RF screens separating the pump from the beam [24]. These pumps were very effective in maintaining a low vacuum pressure until we discovered that some of the RF screens were too thin and were allowing HOM power into the pumping chambers. The NEG material is very lossy and ended up absorbing all of the HOM power. At a LER beam current of 2.2 A and with a bunch length of about 10–12 mm we found that certain NEG pumps located about 50 m upstream of the detector were absorbing enough RF power to achieve regeneration temperatures (nearly 400 °C). Initially, we had no temperature information on the NEG pumps and had no idea any of the pumps were getting hot. NEG pumps start outgassing at temperatures significantly below regeneration temperatures (see Fig. 41) and this region of the accelerator relied almost exclusively on NEG pumping so there were only a few ion pumps in the upstream 70 m from the IP.

If a hot NEG had a nearby NEG that was staying cool we had no indication of a pressure increase as the cool NEG would pump out the gas from the hot NEG before any ion pump would see the pressure rise. Hence, greatly increased detector backgrounds were the first sign of a vacuum problem in this area.

Fig. 42 shows a temperature rise for a NEG pump in the upstream LER and Fig. 43 is a plot of the LER beam current over the same time period.

Depending on the vacuum chamber design and on the space available, several different pumping chambers and RF screens

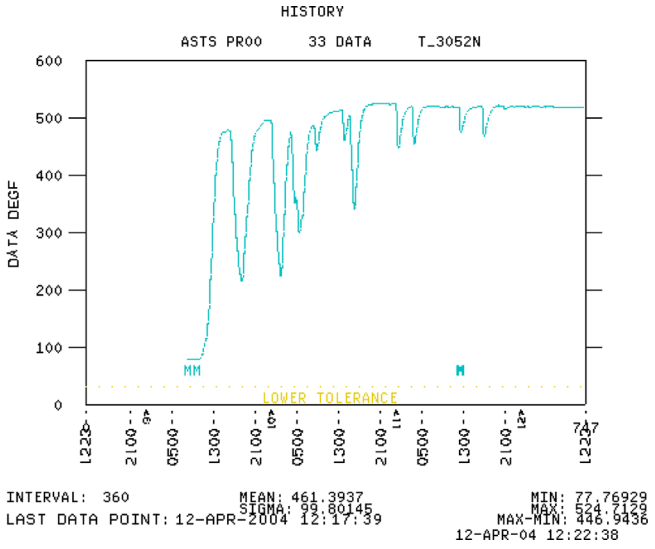

Fig. 42. This particular NEG pump achieved a temperature in excess of 500 °F (260 °C). Note the very long time scale of the heating. The plot is over about 3 days of beam time. The long time scale was one of the reasons this problem was difficult to uncover.

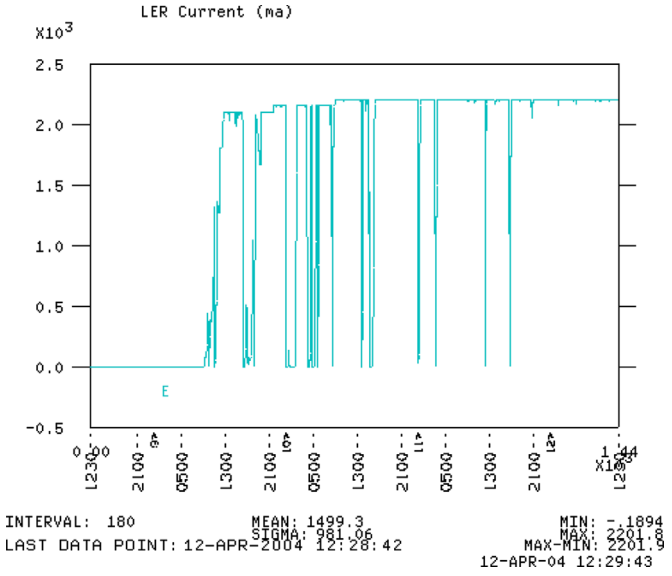

Fig. 43. The LER beam current over the same time period as in Fig. 41. Note the decreases in the NEG temperature coincide with extended periods when there was no LER beam.

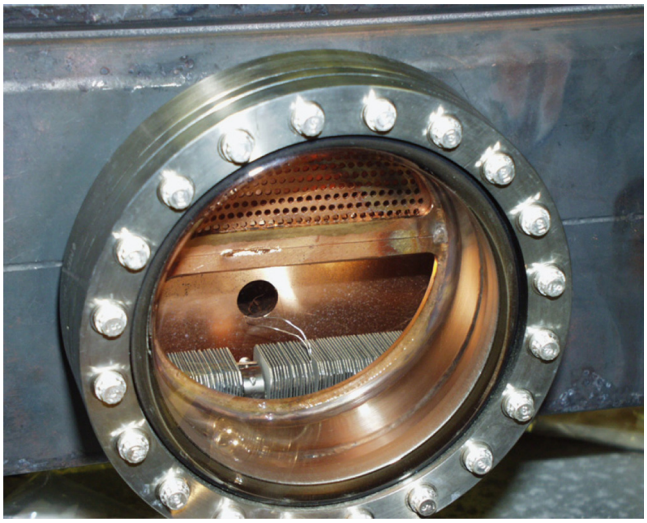

Fig. 44. Test module for the NEG pump. The wires leading from the pump material are a thermocouple.

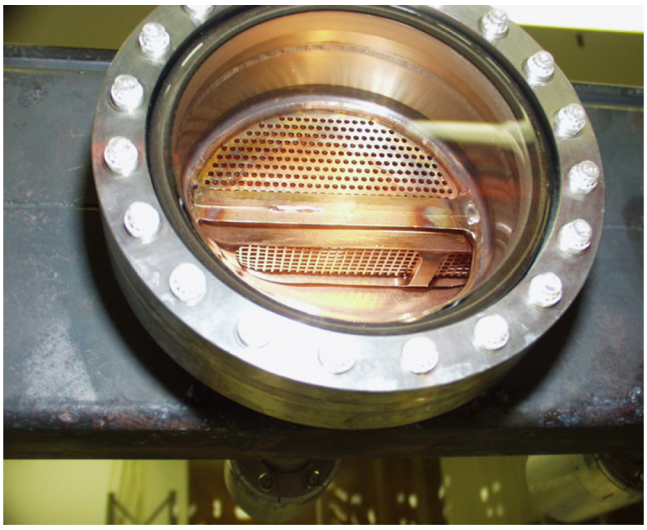

Fig. 45. The same chamber showing two different screen designs. The more difficult screen to see is a square hole design that proved to be more susceptible to letting HOM power into the pumping chamber.

were employed. Studies of NEG temperature increases indicated that essentially all screen designs were letting some amount of RF power into the pumping chamber but that some were very much worse than others. Modest HOM power leakage was OK as long as the NEG temperature did not get too high.

The NEG pumps were thermally isolated from the water-cooled Cu vacuum chamber as much as possible in order to be able to heat the pumps to regeneration temperatures. This meant that small amounts of RF power (10–50 W) was more than enough to heat the NEG pumps up to very high temperatures.

An analysis of the temperature data (obtained by inserting a thermocouple into the tube containing the heater rod for pump regeneration) led to the conclusion that screen designs where long z slots had been cut through the beam pipe wall with a thin copper mesh tacked to the wall on the pumping side of the slots were the least effective in blocking out the HOM power.

A general conclusion reached after studying all of the various screens was that a good RF screen had to have a minimum hole depth through the screen material (generally Cu or Al) that was at least equal to the diameter of the hole. Even with this design, HOM power could begin to penetrate into the pumping chamber if there were local discontinuities that were generating high frequency HOM power. More hole depth is needed to suppress higher frequency HOM power but this then tends to limit the amount of available pumping. Fig. 44 shows a typical NEG pump used in the interaction region area and Fig. 45 shows two examples of screens.

Acknowledgments

The authors would like to thank the PEP-II physicists, operators and engineers of the Accelerator Department for their consistent help with understanding and solving these problems and especially S. Ecklund, A. Kulikov, U. Wienands, F.-J. Decker, S. Weathersby S. DeBarger, N. Kurita, S. Metcalfe, J. Langton, N. Reeck, M. Kosovsky, J. Defever, A. Sheng and D. Wright. This work was supported by Department of Energy Contract No. DOE-AC03–76SF00515.

References

[1] J. Seeman, Last year of PEP-II B-factory Operation, EPAC 2008, p. 946.
[2] S. Ecklund, et al., High Order Mode Heating Observations, PAC 2001, p. 3576.
[3] A. Novokhatski, S. Weathersby, RF Modes in the PEP-II Shielded Vertex Bellows, PAC 2003.
[4] C.-K. Ng, N. Folwell, L. Ge, J. Langton, L.-Q. Lee, A. Novokhatski, Simulation of HOM Leakage in the PEP-II Bellows, PAC 2003, TPPP028.
[5] S. Weathersby, J. Langton, A. Novokhatski, J. Seeman, Damping Higher Order Modes in the PEP-II B-Factory Vertex Bellows, PAC 2005, TPPP030.
[6] A. Novokhatski, J..Seeman, M..Sullivan, RF Heating and Temperature Oscillations due to a Small Gap in a PEP-II Vacuum Chamber, PAC 2003, WPG014.
[7] U. Wienands, et al., Tracking Down a Fast Instability in the PEP-II LER, EPAC 2006, MOPLS051.
[8] A. Novokhatski, J. Seeman, M. Sullivan, Radiolocation of a HOM Source in the PEP-II Rings, EPAC 2008, TUPPO53.
[9] A. Novokhatski, HOM Effects in Vacuum System with Short Bunches, PAC'05, Knoxville, Tennessee, USA, May 2005, p. 289.
[10] N. Kurita, et al., Numerical Simulation of the PEP-II Beam Position Monitor, SLAC-PUB-95–7006, September 1995.
[11] S. Weathersby, A. Novokhatski, BPM Breakdown Potential in the PEP-II B-Factory Storage Ring Collider, ICAP 2009, THPSC058.
[12] A. Novokhatski, et al., Damping the Higher Order Modes in the Pumping Chamber of the PEP-II Low Energy Ring, EPAC 2004, MOPLT135.
[13] A. Novokhatski, J. Seeman, S. Weathersby, Physical Review Special Topics – Accelerators and Beams 10 (2007) 042003.
[14] U. Wienands, et al., A Transverse Beam Instability in the PEP-II HER Induced by Discharges in the Vacuum System, PAC07-TUPAS068.
[15] A. Novokhatski, J. Seeman, M. Sullivan, A Model of an Electrical Discharge in the Flange Contacts with Omega Seals at High Currents in PEP-II, EPAC 2008, TUPP054.
[16] A. Novokhatski, The Computer Code NOVO for the Calculation of Wake Potentials of the Very Short Ultra-relativistic Bunches, SLAC-PUB-11556, December 2005.
[17] M. Sullivan, et al., Anomalous High Radiation Beam Aborts in the PEP-II B-factory, EPAC 06, Edinburgh, June 2006, p. 652.
[18] A. Novokhatski, J. Seeman, M. Sullivan, Modelling of the Sparks in Q2-Bellows, PAC 2007, FRPM075.
[19] A. Burov, A. Novokhatski, Wake potential of a dielectric canal, in: Proceedings of HEACC'92, Hamburg, Germany, 1992, p. 537.
[20] A. Novokhatski, et al., A New Q2-Bellows Absorber, PAC 2007, FRMS076.
[21] A. Novokhatski, Overall HOM Measurement at High Beam Currents in the PEP-II SLAC B-Factory, PAC 2007, p. 45.
[22] A. Novokhatski, M. Sullivan, Loss Factor of the PEP-II Rings, EPAC2008, p. 1670.
[23] S. Heifets, C.K. Ng, A. Novokhatski, S. Weathersby, Review of Impedance Issues for B-Factory, SLAC-PUB-10837, November 2004.
[24] L. Bertolini, et.al., Design of the Linear Non-Evaporable Getter Pump for the PEP-II B-Factory, PAC 1997, 3622.